Acta Biomaterialia 99 (2019) 443–456

Contents lists available at ScienceDirect

Acta Biomaterialia

journal homepage: www.elsevier.com/locate/actbio

Full length article

Failure properties and microstructure of healthy and aneurysmatic human thoracic aortas subjected to uniaxial extension with a focus on the media

Selda Sherifova[a], Gerhard Sommer[a], Christian Viertler[b], Peter Regitnig[b], Thomas Caranasos[c], Margaret Anne Smith[d], Boyce E. Griffith[e], Ray W. Ogden[f], Gerhard A. Holzapfel[a,g,*]

[a] Institute of Biomechanics, Graz University of Technology, Austria
[b] Diagnostic and Research Institute of Pathology, Medical University of Graz, Austria
[c] Division of Cardiothoracic Surgery, University of North Carolina at Chapel Hill, USA
[d] Carolina Center for Interdisciplinary Applied Mathematics, University of North Carolina at Chapel Hill, USA
[e] Department of Mathematics, University of North Carolina at Chapel Hill, USA
[f] School of Mathematics and Statistics, University of Glasgow, UK
[g] Department of Structural Engineering, Norwegian Institute of Science and Technology (NTNU), Trondheim, Norway

ARTICLE INFO

Article history:
Received 8 May 2019
Revised 14 August 2019
Accepted 21 August 2019
Available online 26 August 2019

Keywords:
Human thoracic aorta
Aneurysm rupture
Dissection
Tissue failure
Uniaxial extension testing
Second-harmonic imaging
Histology
Collagen microstructure

ABSTRACT

Current clinical practice for aneurysmatic interventions is often based on the maximum diameter of the vessel and/or on the growth rate, although rupture can occur at any diameter and growth rate, leading to fatality. For 27 medial samples obtained from 12 non-aneurysmatic (control) and 9 aneurysmatic human descending thoracic aortas we examined: the mechanical responses up to rupture using uniaxial extension tests of circumferential and longitudinal specimens; the structure of these tissues using second-harmonic imaging and histology, in particular, the content proportions of collagen, elastic fibers and smooth muscle cells in the media. It was found that the mean failure stresses were higher in the circumferential directions (Control-C 1474 kPa; Aneurysmatic-C 1446 kPa), than in the longitudinal directions (Aneurysmatic-L 735 kPa; Control-L 579 kPa). This trend was the opposite to that observed for the mean collagen fiber directions measured from the loading axis (Control-L > Aneurysmatic-L > Aneurysmatic-C > Control-C), thus suggesting that the trend in the failure stress can in part be attributed to the collagen architecture. The difference in the mean values of the out-of-plane dispersion in the radial/longitudinal plane between the control and aneurysmatic groups was significant. The difference in the mean values of the mean fiber angle from the circumferential direction was also significantly different between the two groups. Most specimens showed delamination zones near the ruptured region in addition to ruptured collagen and elastic fibers. This study provides a basis for further studies on the microstructure and the uniaxial failure properties of (aneurysmatic) arterial walls towards realistic modeling and prediction of tissue failure.

Statement of Significance

A data set relating uniaxial failure properties to the microstructure of non-aneurysmatic and aneurysmatic human thoracic aortic medias under uniaxial extension tests is presented for the first time. It was found that the mean failure stresses were higher in the circumferential directions, than in the longitudinal directions. The general trend for the failure stresses was Control-C > Aneurysmatic-C > Aneurysmatic-L > Control-L, which was the opposite of that observed for the mean collagen fiber direction relative to the loading axis (Control-L > Aneurysmatic-L > Aneurysmatic-C > Control-C) suggesting that the trend in the failure stress can in part be attributed to the collagen architecture. This study provides a first step towards more realistic modeling and prediction of tissue failure.

* Corresponding author at: Institute of Biomechanics, Graz University of Technology, Austria.
E-mail address: holzapfel@tugraz.at (G.A. Holzapfel).

https://doi.org/10.1016/j.actbio.2019.08.038
1742-7061/

1. Introduction

Aneurysms and dissections of thoracic aortas are life threatening conditions with high mortality rates even though clinical procedures have been improved in recent years [1–3]. Current practice guidelines recommend surgical repair of large thoracic aortic aneurysms (with maximum diameter of the lesion of 5.0 cm in women or 5.5 cm in men or if the maximum diameter increases more than 0.5–1.0 cm in one year [4–6]) to prevent fatal aortic dissection or rupture, but observations have shown that adverse aortic events may already occur at smaller diameters [7]. Interestingly, more than 80% of aortic dissections develop in the absence of a pre-existing aneurysm, indicating that aneurysm formation and dissection are in general different pathophysiological conditions [8]. Since there is a variety of causes for the development of thoracic aortic diseases, a greater knowledge of patient-specific biomechanical properties reflecting the influence of the microstructure is important for predicting adverse events.

The healthy thoracic aorta has a unique structural composition that enables it to withstand the large tissue stresses created mainly by the blood pressure [9]. Of the three main layers, the innermost layer, the intima, consists of a single layer of endothelial cells in a healthy young artery, and its solid mechanical contribution is negligible [10]. However, intimas, especially from older patients, often exhibit a considerable thickening due to intimal hyperplasia, fibrosis and sclerotic changes, and therefore have a significant solid mechanical influence [11]. The medial layer is responsible for the main structural and functional properties of the thoracic aorta [12,13]. It consists of many medial lamellar units each having a thickness of about 13-15 μm, with smooth muscle cells in the lamellar unit interconnecting the elastic laminas, and interspersed collagen fibers (mostly of type I and III) [14]. The outer layer, the adventitia, consists mainly of thick bundles of wavy collagen fibers (mostly type I) in the unloaded state, and is therefore very compliant at small strains but changes to a stiff 'jacket-like' tube at high strains so that the artery is prevented from overstretching and rupture [10,11,15]. Schriefl et al. [16] described the media and the adventitia of aged thoracic aortas as displaying two collagen fiber families organized in separate sublayers with different orientations. The media incorporates two symmetric fiber families with mean fiber angles closer to the circumferential direction, while the adventitial layer has collagen fibers oriented closer to the longitudinal direction. In the intima, however, this organization in layers is less clear with sometimes a third or a fourth family of fibers being apparent, and in general displaying a carpet-like structure [16].

Pathological changes leading to dissection and aneurysm formation in the thoracic aorta typically alter the microstructure and weaken the media. Medial degeneration (cystic medial necrosis) is a characteristic of dissections and it involves smooth muscle cell loss, elastic fiber fragmentation and accumulation of glycosaminoglycans [17–20]. A weakened aortic wall due to medial degeneration is also typical for aneurysms and aneurysms combined with dissections of the ascending thoracic aorta [21]. Although similar collagen contents were observed in control and aneurysm samples [22], the organization of collagen may nevertheless be significantly changed during aneurysm development in the thoracic aorta [23]. An increased collagen content [24–26] or a decreased collagen content with increased disruption were reported for aortic dissections [21,23]. Thus, pathological changes are often said to weaken the aortic wall, thereby increasing the likelihood of rupture.

Fig. 1 shows two aortic medial specimens with different collagen microstructures cut out from adjacent regions. As is well-known fibrillar collagen plays an important reinforcing role in fibrous tissues and the mechanical properties of the tissues are significantly different in directions along and orthogonal to the mean collagen fiber direction. This motivated the present study of the failure properties of control and aneurysmatic human thoracic aortic medias. These were investigated using uniaxial extension tests in the circumferential and longitudinal directions. The mechanical testing was combined with second-harmonic generation imaging and histological investigations to study the influence of the collagen architecture on the mechanical failure properties.

2. Materials and methods

Control samples were obtained from non-aneurysmatic human descending thoracic aortas ($n = 12$) by the Diagnostic and Research Institute of Pathology, Medical University of Graz, Austria. Aneurysmatic samples ($n = 9$) were obtained from patients undergoing ascending aortic surgical repair at the Division of Cardiac Surgery, Medical University of Graz, Austria and the Division of Cardiothoracic Surgery, University of North Carolina at Chapel Hill (UNC). The use of the donor samples was approved by the local Ethics Committee at the Medical University of Graz (27–250 ex 14/15) and the University of North Carolina at Chapel Hill Institutional Review Board (Study No. 14-2529). For the aneurysmatic samples, informed consents were obtained prior to sample collection. Upon explantation, donor samples obtained from the Medical University of Graz were placed in phosphate buffered saline (PBS) prior to freezing, whereas donor samples from UNC were placed into a tube containing Ringer's lactate with 10% dimethyl sulfoxide (DMSO) to preserve mechanical properties during transportation. This tube was placed in another container filled with isopropanol solution which was surrounded by dry ice to ensure slow freezing. Samples were placed in a freezer at −24°C upon arrival and kept therein until testing for varying time periods (minimum = 8, maximum = 154 days).

2.1. Mechanical testing

Following unfreezing overnight at 4 °C, each donor sample was cut open along its longitudinal axis, and separated into intimal, medial and adventitial layers using scalpel and scissors; Fig. 2(a) and (b). Dog-bone shaped specimens were then punched out from the circumferential and longitudinal directions of each sample using a template; see Fig. 2(c). After the initial thickness T was measured optically using the system described in [27], for each specimen black markers were placed approximately 5 mm apart on the gage region for video tracking, and the specimen was then mounted on the apparatus. The initial length L and width W values were then measured using the videoextensometer described in [28]. Each specimen was preconditioned to 50 kPa (engineering stress) in five loading-unloading cycles. Subsequently, control and aneurysmatic specimens in the circumferential and longitudinal directions were extended until failure quasi-statically with a cross-head speed of 2 mm/min. The testing protocol was similar to that used in [29–31] and took place in a PBS filled container heated up to and maintained at 37 °C. Tests were regarded as unsuccessful if failure occurred outside the markers, and the results for these cases were discarded; see Fig. 2(d) and (e) for a successful and an unsuccessful test, respectively. After a successful test, the specimen was fixed in 4% formaldehyde in preparation for microstructural investigations.

The uniaxial Cauchy stress σ and the related stretch λ were calculated for each specimen using the force-displacement data from the formulas $\sigma = \lambda F/A$, where F is the measured force, $A = TW$ the initial cross-sectional area, while $\lambda = 1 + d/L$, where d is the measured displacement and L is the initial length. The failure stress σ_f

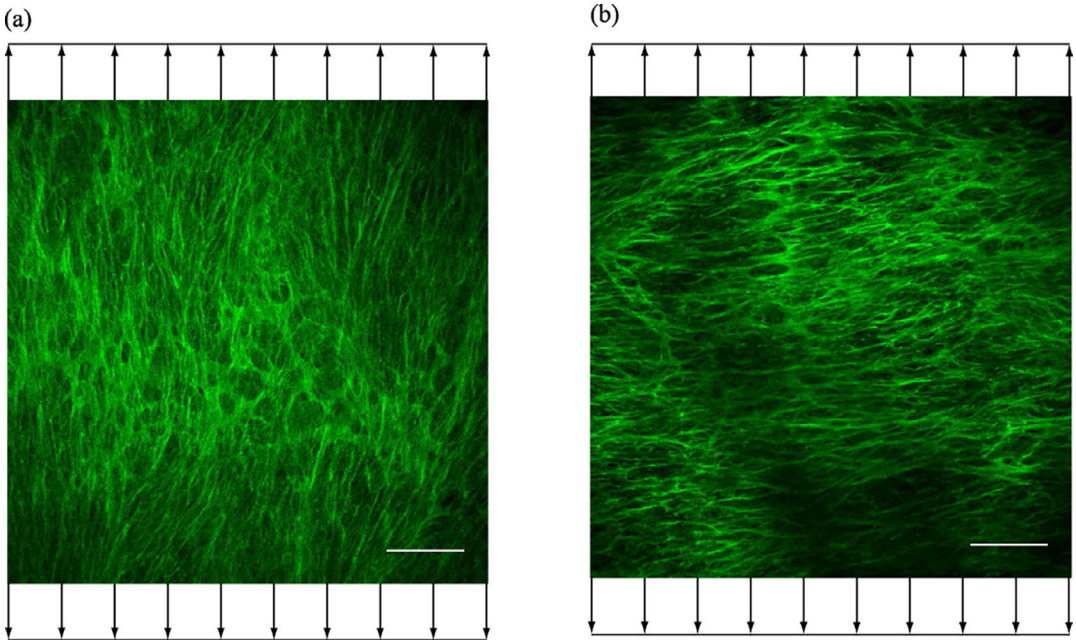

Fig. 1. Second-harmonic generation images of two aortic medial specimens cut out from adjacent regions: (a) load applied along the main direction of fiber reinforcement for a circumferential specimen; (b) load applied orthogonal to the main direction of fiber reinforcement for a longitudinal specimen. Collagen fibers are represented in green, while the arrows indicate the direction of the load. Images were enhanced for visualization. White scale bars correspond to 100 μm.

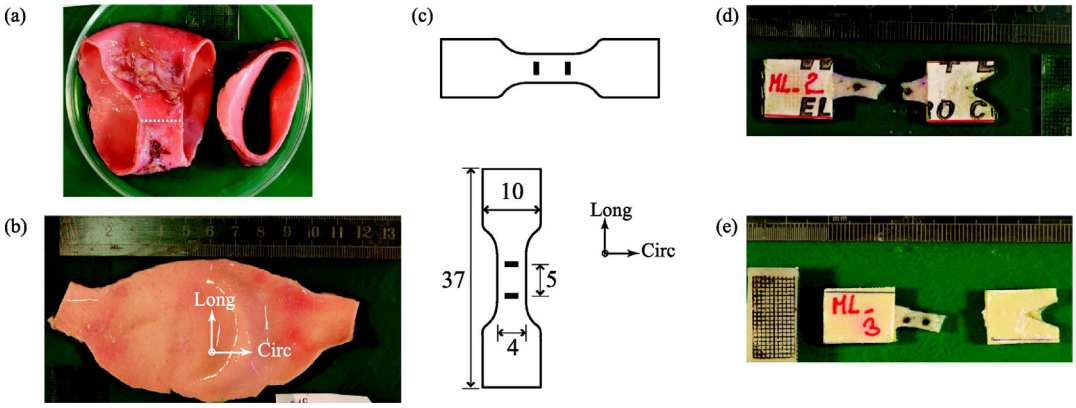

Fig. 2. Sample preparation, template and examples of rupture in uniaxial tests: (a) donor sample ready to be cut open along its longitudinal axis indicated by the dotted white line; (b) media of the sample after cutting open and separation of the layers; (c) schematic of dog-bone shaped template in the circumferential and longitudinal directions with black markers placed approximately 5 mm apart for video tracking; (d) and (e) examples of a successful and an unsuccessful test, respectively. The included millimeter scale provides a dimensional reference.

was defined to be the value of the Cauchy stress at the maximum force. The corresponding stretch at failure is denoted by λ_f.

2.2. Microstructural investigations

Half of the successful test specimens were optically cleared for subsequent second-harmonic generation (SHG) imaging in graded ethanol series and a solution of benzyl alcohol to benzyl benzoate (BABB), as described in [32]. The imaging set-up was the same as in [32] except that the in-plane image stacks in the circumferential-longitudinal plane CL (θz) were acquired using $620 \times 620 \times 5\,\mu$m sampling instead of $620 \times 620 \times 1\,\mu$m. The out-of-plane images were acquired from the radial-circumferential plane RC ($r\theta$) and radial-longitudinal plane RL (rz) orthogonal to the RC plane. Note that the word 'fiber' in mean fiber angle and in fiber dispersion refers to 'collagen fiber'.

Following the SHG imaging, image stacks of the CL plane were used to obtain the mean fiber angle α, measured with respect to the circumferential direction. Note that the mean fiber angle from the specimen loading axis corresponds to α and $90° - \alpha$ for the circumferential and longitudinal test specimens, respectively. The fiber dispersion parameter κ_{ip} in the (θz) plane is given by the formula

$$\kappa_{ip} = \frac{1}{2} - \frac{I_1(a)}{2I_0(a)}, \tag{1}$$

where I_0 and I_1 are the modified Bessel functions of the first kind of order 0 and 1, respectively, while a is a concentration parameter from the von Mises distribution [33] obtained using maximum likelihood estimation. The corresponding out-of-plane fiber dispersion parameters $\kappa_{op}^{r\theta}$ and κ_{op}^{rz} were calculated according to

$$\kappa_{op} = \frac{1}{2} - \frac{1}{8b} + \frac{1}{4}\sqrt{\frac{2}{\pi b}}\frac{\exp(-2b)}{\mathrm{erf}(\sqrt{2b})}, \tag{2}$$

which is again based on the von Mises distribution, erf being the error function defined by [33]

$$\mathrm{erf}(x) = \frac{2}{\sqrt{\pi}}\int_0^x \exp(-\xi^2)\mathrm{d}\xi. \tag{3}$$

Images from the RC and RL planes were used to obtain the concentration parameter b via least-square fitting. This distribution function is evaluated with a different concentration parameter b for the two planes $r\theta$ and rz. Note that $\kappa_{\text{op}}^{r\theta}$ and κ_{op}^{rz} relate to the $(r\theta)$ and (rz) planes. An indication of the four structural parameters $\alpha, \kappa_{\text{ip}}, \kappa_{\text{op}}^{rz}$ and $\kappa_{\text{op}}^{r\theta}$ relative to the coordinate system r, θ, z can be found in Fig. 3.

The other half of the specimens were used to obtain whole slide histological images. The clamped ends of the specimens were marked with a dye prior to paraffin embedding to distinguish the rupture zone (area near the ruptured end) for qualitative evaluations. Following the paraffin embedding, Hematoxylin and Eosin (H&E) staining was performed together with Elastica van Gieson (EvG) on adjacent sections for the identification of collagen, elastic fibers (with all their proteins, not only elastin [34], p. 1065; for an instructive illustration see Fig. 1 in [20]) and smooth muscle cell (SMC) nuclei. Whole histological slides were scanned using a 3DHISTECH P1000 slide scanner (3DHISTECH Ltd., Budapest, Hungary), and the whole slide images were subsequently evaluated using the software CaseViewer (v2.1; 3DHISTECH Ltd., Budapest, Hungary). In particular, the specimens from the successful tests were quantified for collagen, elastic fibers and SMC content (total content 100%), without taking the ground substance into account. Content evaluations were performed independently by two experienced pathologists in a semiquantitative manner. In addition, the thickness of the media was evaluated as a percentage of the specimen thickness, and possibly attached layers despite the separation such as the intima and the adventitia were identified.

2.3. Statistics

The one-way analysis of variance (ANOVA) followed by Tukey's test was employed for statistical analysis. More specifically, the structural parameters $\alpha, \kappa_{\text{ip}}, \kappa_{\text{op}}^{r\theta}, \kappa_{\text{op}}^{rz}$, as well as collagen, elastic fiber and SMC content percentages were compared between the control and the aneurysmatic groups of specimens. In addition, the mechanical failure parameters $\sigma_{\text{f}}, \lambda_{\text{f}}$, the structural parameters, and the content percentages were compared between the four groups (Control-C/Control-L and Aneurysmatic-C/Aneurysmatic-L). The groups were significantly different if $p < 0.05$. Mean ($\pm$ standard deviation), median, first and third quartile values $(\text{Q1}, \text{Q3})$ of the aforementioned groups were computed. Linear regression was performed to see if there was any correlation between failure stress and failure stretch, and failure stress/failure stretch and aneurysm diameter. Only the specimens for which the media constituted at least 75% of the total thickness were included in the statistics, because the main focus of the present study is a comparison of medial mechanics and structure.

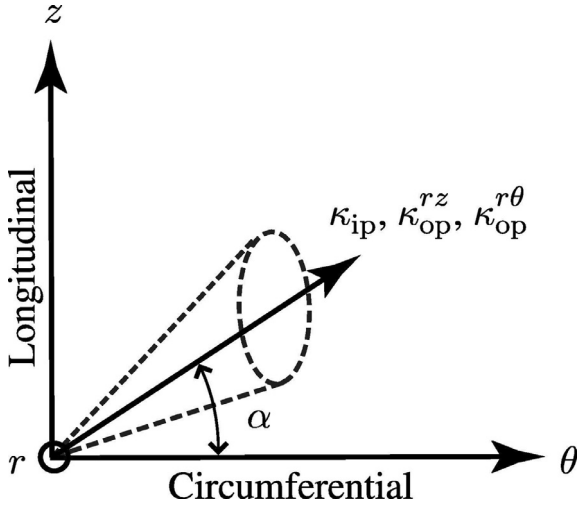

Fig. 3. Illustration of four structural parameters $\alpha, \kappa_{\text{ip}}, \kappa_{\text{op}}^{rz}$ and $\kappa_{\text{op}}^{r\theta}$ with respect to the coordinate axes, r (radial), θ (circumferential) and z (longitudinal). The mean fiber direction is denoted by the solid line with the arrow located in the (θz) plane, and making an angle α with the circumferential direction.

3. Results

Table 1 depicts the anamnesis of all donors labeled by C_{I}–C_{XII} for control and A_{I}–A_{IX} for aneurysmatic specimens. In total 27 uniaxial tests (Control-C, $n = 7$; Control-L, $n = 10$; Aneurysmatic-C, $n = 4$; Aneurysmatic-L, $n = 6$) from 21 thoracic aortas (Control $n = 12$, Aneurysmatic $n = 9$) were included. Table 2 contains a summary of the following values: the failure stress σ_{f} and the failure stretch λ_{f}; the structural parameters $\alpha, \kappa_{\text{ip}}, \kappa_{\text{op}}^{r\theta}, \kappa_{\text{op}}^{rz}$; the collagen, elastic fiber and SMC content percentages; the thickness of the media after layer separation as a percentage of the whole specimen thickness; and the identification of the layers which remain attached after the separation.

3.1. Mechanical testing

Table 3 provides a summary for the mean, median and $(\text{Q1}, \text{Q3})$ values of the mechanical and structural data, and the collagen, elastic fibers and SMC content percentages of the four groups from Table 2 with exclusion of the specimens: circumferential C_{III}, circumferential and longitudinal C_{X} and circumferential A_{I}. With reference to Table 3 the Control-C group showed the highest mean failure stress σ_{f} (1474 ± 1131 kPa), followed by Aneurysmatic-C (1446 ± 875 kPa), Aneurysmatic-L (735 ± 227 kPa) and Control-L (579 ± 172 kPa). The groups were not significantly different. From Table 2 it can be seen that the highest failure stress value is for the circumferential specimen C_{IV} (3418 kPa), whereas the lowest value was observed for the longitudinal specimen C_{I} (222 kPa).

Control-C showed the highest mean failure stretch λ_{f} (2.18 ± 0.87) followed by Aneurysmatic-L (1.6 ± 0.22), Control-L (1.9 ± 0.46) and Aneurysmatic-C (1.59 ± 0.07), see Table 3. There were no significant differences between the groups. The highest failure stretch value λ_{f} was observed for the circumferential specimen C_{IV} (3.2), whereas the lowest was observed for the circumferential specimen A_{I} (1.17), see Table 2.

The Cauchy stress versus stretch plots for the specimens of the four groups are depicted in Fig. 5, but the failure stress σ_{f} revealed no significant correlation with the failure stretch λ_{f}, as shown in Fig. 6. It was found that the aneurysm diameter did not correlate with either failure stress or failure stretch.

3.2. Microstructural investigations

3.2.1. Second-harmonic generation

Table 4 summarizes the mean, median and $(\text{Q1}, \text{Q3})$ values of the structural data from Table 2 for the control specimens and separately for the aneurysmatic specimens with more than 75% of the media present. The mean fiber direction α is closer to the circumferential direction and more aligned for the control specimens ($\alpha = 15° \pm 8°, \kappa_{\text{ip}} = 0.23 \pm 0.04$) than for the aneurysmatic specimens ($\alpha = 22° \pm 9°, \kappa_{\text{ip}} = 0.24 \pm 0.06$). The means of the two groups were significantly different for α ($p = 0.0496$) but not for κ_{ip} ($p = 0.743$). Mean values for the out-of-plane dispersions in each plane were higher for control ($\kappa_{\text{op}}^{r\theta} = 0.48 \pm 0.02, \kappa_{\text{op}}^{rz} = 0.48 \pm 0.01$) compared to aneurysmatic ($\kappa_{\text{op}}^{r\theta} = 0.47 \pm 0.01, \kappa_{\text{op}}^{rz} = 0.45 \pm 0.02$); but the difference was significant only in the rz plane ($p < 0.001$).

Table 1
Anamnesis of donors for control (C_I–C_{XII}) and aneurysmatic (A_I–A_{IX}) specimens including the cause of death (COD) for the control, risk factors, age and gender. Samples were provided by the Medical University of Graz (MUG) and the University of North Carolina at Chapel Hill (UNC).

Donor	Hospital	COD	Risk Factors	Age	Gender
C_I	MUG	Myocardial infarction	–	59	m
C_{II}	MUG	Tumor progression	–	56	f
C_{III}	MUG	Myocardial infarction	D, HL, HT, SM	68	m
C_{IV}	MUG	Metastasis	–	59	f
C_V	MUG	Multiorgan failure, sepsis	–	52	f
C_{VI}	MUG	Tumor progression	D, HT	83	m
C_{VII}	MUG	Tumor progression	–	69	f
C_{VIII}	MUG	Cardiogenic shock	–	65	f
C_{IX}	MUG	Epileptic shock	–	19	m
C_X	MUG	Tumor progression	HT	65	f
C_{XI}	MUG	High brain pressure	HT	68	f
C_{XII}	MUG	Aspiration	–	52	m
A_I	MUG	–	D, HL, HT, SM, KI	66	m
A_{II}	UNC	–	UAV, GERD, AI, AS	51	m
A_{III}	UNC	–	UAV, AI, AS, HL, LVH	56	m
A_{IV}	UNC	–	HT	68	m
A_V	UNC	–	AS, AI, BAV, GERD, O	45	m
A_{VI}	UNC	–	HT	63	m
A_{VII}	UNC	–	GERD, O	71	f
A_{VIII}	UNC	–	ED, HT, SM	46	f
A_{IX}	UNC	–	AI, AR, HFrEF	44	m

AI, aortic insufficiency; AR, aortic regurgitation; AS, aortic stenosis; BAV, biscuspid aortic valve; D, diabetes; ED, Ehlers-Danlos syndrome; GERD, gastroesophageal reflux disease; HFrEF, heart failure with reduced ejection fraction; HL, hyperlipidemia; HT, hypertension; KI, kidney insufficiency; LVH, left ventricular hypertrophy; O, obesity; SM, smoking; UAV, unicuspid aortic valve.

Table 2
Overview of the failure properties, the structural parameters, the content percentages for collagen, elastic fibers and SMC, the thickness of the media, and the visible layers for each specimen identified.

Donor	C/L	σ_f [kPa]	λ_f [–]	α [°] [–]	κ_{ip} [–]	$\kappa_{op}^{r\theta}$ [–]	κ_{op}^{rz} [%]	Collagen [%]	Elastic fibers [%]	SMC [%]	Thickness of media [%]	Visible layers
C_{III}	C	1200	1.39	43	0.20	0.49	0.47	30	30	40	65	IM
C_{IV}	C	3418	3.20	7	0.20	0.49	0.49	30	30	40	80	MA
C_V	C	1502	2.03	17	0.32	0.49	0.45	30	30	40	87	IM
C_{VII}	C	848	1.42	12	0.24	0.48	0.49	25	40	35	100	M
C_{VIII}	C	655	1.30	33	0.23	0.48	0.49	30	40	30	76	IM
C_{IX}	C	948	2.97	24	0.29	0.41	0.49	25	45	30	100	M
C_X	C	1541	1.59	20	0.22	0.48	0.48	30	30	40	71	IM
C_I	L	222	1.77	11	0.20	0.48	0.46	20	30	50	100	M
C_{II}	L	679	2.41	11	0.21	0.48	0.48	25	40	35	100	M
C_{III}	L	776	1.23	15	0.18	0.49	0.49	20	30	50	76	IM
C_{IV}	L	750	2.14	9	0.25	0.48	0.49	30	40	30	100	M
C_{VI}	L	413	1.26	20	0.28	0.49	0.49	30	25	45	84	IM
C_{VII}	L	566	1.62	6	0.21	0.49	0.50	40	50	10	100	M
C_{IX}	L	610	2.47	7	0.25	0.49	0.48	30	50	20	100	M
C_X	L	700	1.41	51	0.22	0.49	0.49	20	50	30	62	IM
C_{XI}	L	564	2.16	25	0.19	0.48	0.49	20	30	50	100	M
C_{XII}	L	633	2.02	8	0.23	0.47	0.48	30	40	30	84	MA
A_I	C	297	1.17	48	0.28	0.45	0.47	70	20	10	46	IM
A_{II}	C	2300	1.65	10	0.19	0.48	0.47	25	35	40	100	M
A_{III}	C	1487	1.51	31	0.29	0.47	0.46	25	35	40	100	M
A_{IX}	C	552	1.61	22	0.26	0.46	0.40	50	30	20	84	IM
A_{II}	L	636	1.81	13	0.17	0.48	0.46	20	30	50	100	M
A_{IV}	L	572	1.83	20	0.26	0.46	0.44	35	35	30	85	MA
A_V	L	988	1.95	34	0.35	0.47	0.44	30	30	40	80	MA
A_{VI}	L	501	2.19	24	0.24	0.47	0.47	30	30	40	100	M
A_{VII}	L	666	1.74	31	0.18	0.47	0.46	30	40	30	86	MA
A_{VIII}	L	1046	2.26	14	0.22	0.47	0.46	20	30	50	100	M

C/L, testing direction (circumferential or longitudinal); σ_f, failure stress; λ_f, failure stretch; α, mean fiber angle measured from the circumferential direction; κ_{ip}, fiber dispersion in the θz plane; $\kappa_{op}^{r\theta}$, fiber dispersion in the $r\theta$ plane; κ_{op}^{rz}, fiber dispersion in the rz plane; SMC, smooth muscle cells; M, media; IM, intima-media; MA, media-adventitia.

With reference to Table 3 there were no significant differences in α and κ_{ip} between the four groups; Control-C ($\alpha = 19° \pm 10°$;$\kappa_{ip} = 0.26 \pm 0.05$), Control-L ($\alpha = 13° \pm 6°, \kappa_{ip} = 0.22 \pm 0.04$), Aneurysmatic-C ($\alpha = 21° \pm 11°, \kappa_{ip} = 0.25 \pm 0.05$), Aneurysmatic-L ($\alpha = 23° \pm 8°, \kappa_{ip} = 0.24 \pm 0.07$). The fiber dispersion $\kappa_{op}^{r\theta}$ in the $r\theta$ plane was not significantly different between Control-C (0.47 ± 0.04), Control-L (0.48 ± 0.01), Aneurysmatic-L (0.47 ± 0.01) and Aneurysmatic-C (0.47 ± 0.01). However, κ_{op}^{rz} in the rz plane was significantly lower in Aneurysmatic-C (0.44 ± 0.04) compared to Control-C (0.48 ± 0.02, $p = 0.0456$) and Control-L (0.48 ± 0.01, $p = 0.02$). The mean fiber angle from the loading direction was significantly higher ($p < 0.001$) in the Control-L ($77° \pm 6°$) and

Table 3
Mean, median and (Q1, Q3) of the failure properties σ_f, λ_f, structural parameters $\alpha, \kappa_{ip}, \kappa_{op}^{r\theta}, \kappa_{op}^{rz}$ and collagen, elastic fibers and SMC content percentages of the four groups. The following specimens were excluded from the statistical analysis: circumferential C_{III}, circumferential and longitudinal C_X and circumferential A_I.

		σ_f [kPa]	λ_f [−]	α [°]	κ_{ip} [−]	$\kappa_{op}^{r\theta}$ [−]	κ_{op}^{rz} [−]	Collagen [%]	Elastic fibers [%]	SMC [%]
Control-C	Mean	1474	2.18	19	0.26	0.47	0.48	28	37	35
	SD	1131	0.87	10	0.05	0.04	0.02	3	7	5
	Q1	800	1.39	11	0.22	0.46	0.48	25	30	30
$n = 5$	Median	948	2.03	17	0.24	0.48	0.49	30	40	35
	Q3	1981	3.03	26	0.30	0.49	0.49	30	41	40
Control-L	Mean	579	1.9	13	0.22	0.48	0.48	27	37	36
	SD	172	0.46	6	0.04	0.01	0.01	7	9	14
	Q1	526	1.53	8	0.20	0.48	0.48	20	30	28
$n = 9$	Median	610	2.02	11	0.21	0.48	0.49	30	40	35
	Q3	697	2.22	16	0.25	0.49	0.49	30	43	50
Aneurysmatic–C	Mean	1446	1.59	21	0.25	0.47	0.44	33	33	33
	SD	875	0.07	11	0.05	0.01	0.04	14	3	12
	Q1	785	1.54	13	0.21	0.46	0.42	25	31	25
$n = 3$	Median	1487	1.61	22	0.26	0.47	0.46	25	35	40
	Q3	2097	1.64	29	0.29	0.48	0.47	44	35	40
Aneurysmatic-L	Mean	735	1.6	23	0.24	0.47	0.46	28	33	40
	SD	227	0.22	8	0.07	0.01	0.01	6	4	9
	Q1	572	1.81	14	0.18	0.47	0.44	20	30	30
$n = 6$	Median	651	1.89	22	0.23	0.47	0.46	30	30	40
	Q3	988	2.19	31	0.26	0.47	0.46	30	35	50

σ_f, failure stress; λ_f, failure stretch; α, mean fiber angle from the circumferential direction; κ_{ip}, fiber dispersion in the θz plane; $\kappa_{op}^{r\theta}$, fiber dispersion in the $r\theta$ plane; κ_{op}^{rz}, fiber dispersion in the rz plane; SMC, smooth muscle cell; SD, standard deviation; (Q1, Q3), first and third quartiles.

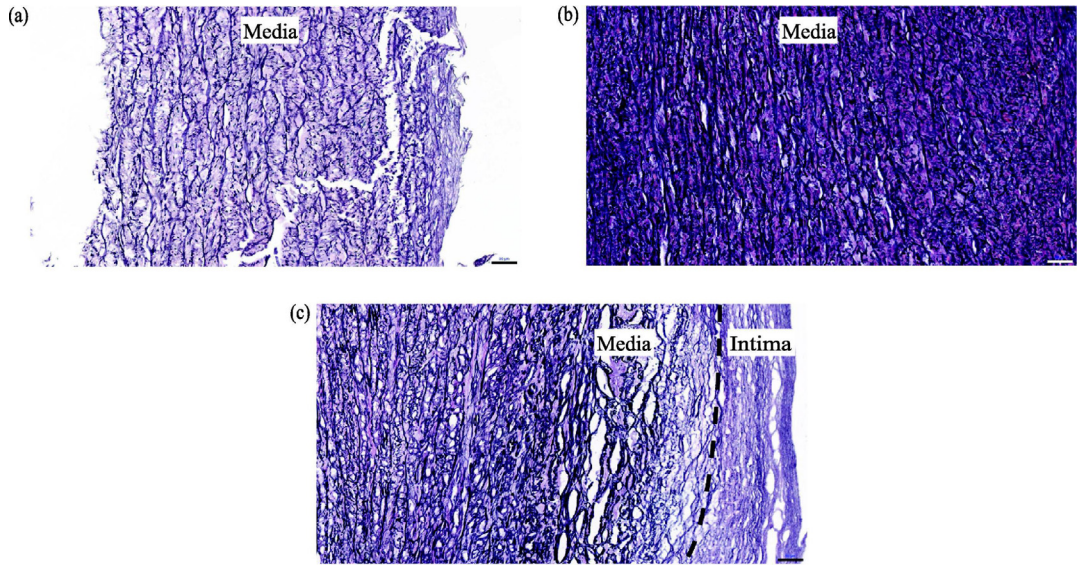

Fig. 4. Representative histological images: (a) longitudinal specimen C_I consisting only of the media; (b) longitudinal specimen C_{II} consisting only of the media; (c) circumferential specimen C_{VIII} indicating presence of the intima. Black and white scale bars correspond to 50 μm.

the Aneurysmatic-L groups ($67° \pm 8°$) than for Control-C ($19° \pm 10°$) and Aneurysmatic-C ($21° \pm 11°$). The general trend, namely highest in Control-L, followed by Aneurysmatic-L, Aneurysmatic-C and Control-C, was the reverse of that for σ_f.

With reference to Table 2, the circumferential specimen C_{IV} and the longitudinal specimen C_{VII} showed the lowest (7°) and highest (84°) angle relative to the loading direction, with similar κ_{ip} of 0.20 and 0.21, respectively. The intensity plots in Fig. 7(a) and (b) depict the fiber architecture of these specimens. The abscissa corresponds to the angle measured from the circumferential direction at the origin (0°), while ±90° refer to the longitudinal direction. The red color identifies fiber angles at which there are fibers with that orientation, while the blue color indicates the absence of fibers. The slightly higher value of κ_{ip} for the specimen C_{VII} is evident from Fig. 7(b). Fig. 7(c) and (d) show the in-plane fiber distributions κ_{ip} of the longitudinal specimens A_{II} ($77°, \kappa_{ip} = 0.17$), and A_{VIII} ($76°, \kappa_{ip} = 0.22$), respectively.

3.2.2. Histology

In regard to Table 4 the mean content percentages of collagen, elastic fibers and SMC were not significantly different between

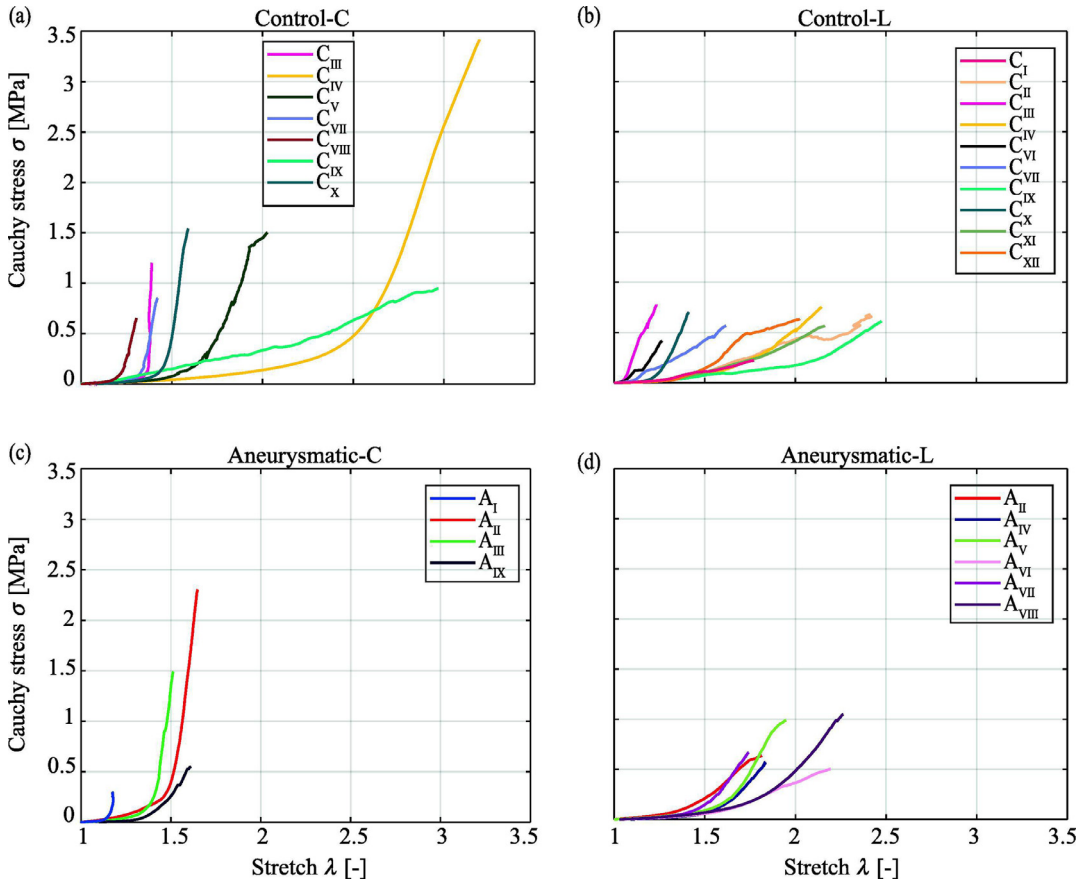

Fig. 5. Cauchy stress σ versus stretch λ plots for all specimens in the circumferential and longitudinal directions: (a) and (b) control group; (c) and (d) aneurysmatic group.

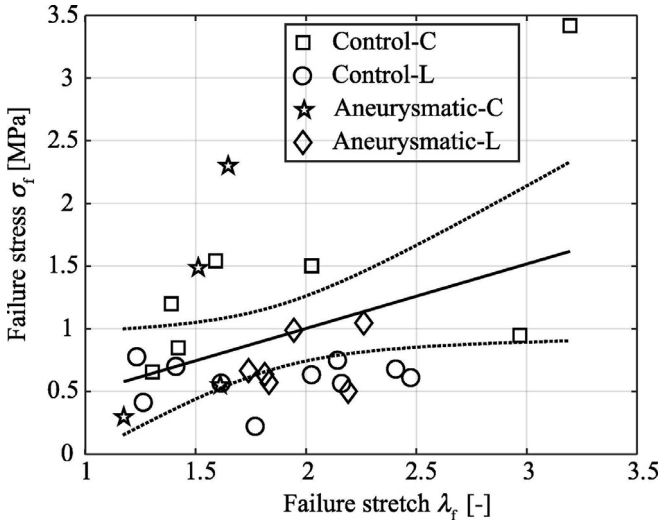

Fig. 6. Failure stress σ_f versus failure stretch λ_f for all the specimens. The solid line corresponds to linear regression with $r^2 = 0.15$. The dotted curves correspond to the confidence bounds.

Control ($28 \pm 5\%$, $37 \pm 8\%$ and $35 \pm 12\%$, respectively) and Aneurysmatic ($29 \pm 9\%$, $33 \pm 4\%$ and $38 \pm 10\%$, respectively). The whole image slides of the specimens did not show significant cystic medial degeneration for aneurysmatic specimens, or freezing artifacts, in general. From Table 3 it can be seen that the mean collagen content was highest in Aneurysmatic-C ($33 \pm 14\%$), followed by Control-C ($28 \pm 3\%$), Aneurysmatic-L ($28 \pm 6\%$) and Control-L ($25 \pm 7\%$). The mean elastic fiber content was similar in Control-L ($37 \pm 9\%$) and Control-C ($37 \pm 7\%$), followed by Aneurysmatic-C ($33 \pm 3\%$) and Aneurysmatic-L ($33 \pm 4\%$). The mean SMC content was highest in Aneurysmatic-L ($40 \pm 9\%$) followed by Control-L ($36 \pm 14\%$), Control-C ($35 \pm 5\%$), and Aneurysmatic-C ($33 \pm 12\%$). The means of the groups were not significantly different for collagen, elastic fiber or SMC contents.

Fig. 4(a) and (b) show the lamellar organization of the media with a disruption (C_I) and with a packed rupture zone (C_{II}), while Fig. 4(c) shows that layer separation was not complete for that particular circumferential specimen (C_{VIII}), see also Table 2 (last column). In regard to Fig. 4 the related colors for collagen, elastic fibers and nuclei are pale pink, black/brown and orange, respectively, while the nuclei can only be seen with a higher magnification. Most specimens showed short or long delamination zones near the ruptured region in addition to ruptured collagen and elastic fibers at the rupture ends, see Fig. 8.

3.3. Uniaxial failure properties and microstructure

Fig. 9(a) and (b) depict the failure stress σ_f and the failure stretch λ_f values in relation to the mean fiber angle relative to the loading direction. While the failure stress exhibits a strong dependence on the mean fiber angle, the failure stretch did not show any such clear dependence. The influences of the fiber dispersion parameters and the collagen, elastic fibers and SMC content percentages on σ_f and λ_f did not show any clear trends.

Table 4
Mean, median and (Q1,Q3) of the structural parameters and content percentages of collagen, elastic fibers and SMC form the Control and the Aneurysmatic groups of specimens obtained from SHG and histology. The following specimens were excluded from the statistical analysis: circumferential C_{III}, circumferential and longitudinal C_X and circumferential A_I.

		α [°]	κ_{ip} [−]	$\kappa_{op}^{r\theta}$ [−]	κ_{op}^{rz} [−]	Collagen [%]	Elastic fibers [%]	SMC [%]
Control	Mean	15	0.23	0.48	0.48	28	37	35
	SD	8	0.04	0.02	0.01	5	8	12
$n = 14$	Median	12	0.23	0.48	0.49	30	40	35
	(Q1,Q3)	(8,20)	(0.20,0.25)	(0.48,0.49)	(0.48,0.49)	(25,30)	(30,40)	(30,45)
Aneurysmatic	Mean	22	0.24	0.47	0.45	29	33	38
	SD	9	0.06	0.01	0.02	9	4	10
$n = 9$	Median	22	0.24	0.47	0.46	30	30	40
	(Q1,Q3)	(14,31)	(0.19,0.27)	(0.46,0.48)	(0.44,0.47)	(24,31)	(30,35)	(30,43)

α, mean fiber angle from the circumferential direction; κ_{ip}, fiber dispersion in the θz plane; $\kappa_{op}^{r\theta}$, fiber dispersion in the $r\theta$ plane; κ_{op}^{rz}, fiber dispersion in the rz plane; SMC, smooth muscle cells; SD, standard deviation; (Q1, Q3), first and third quartiles.

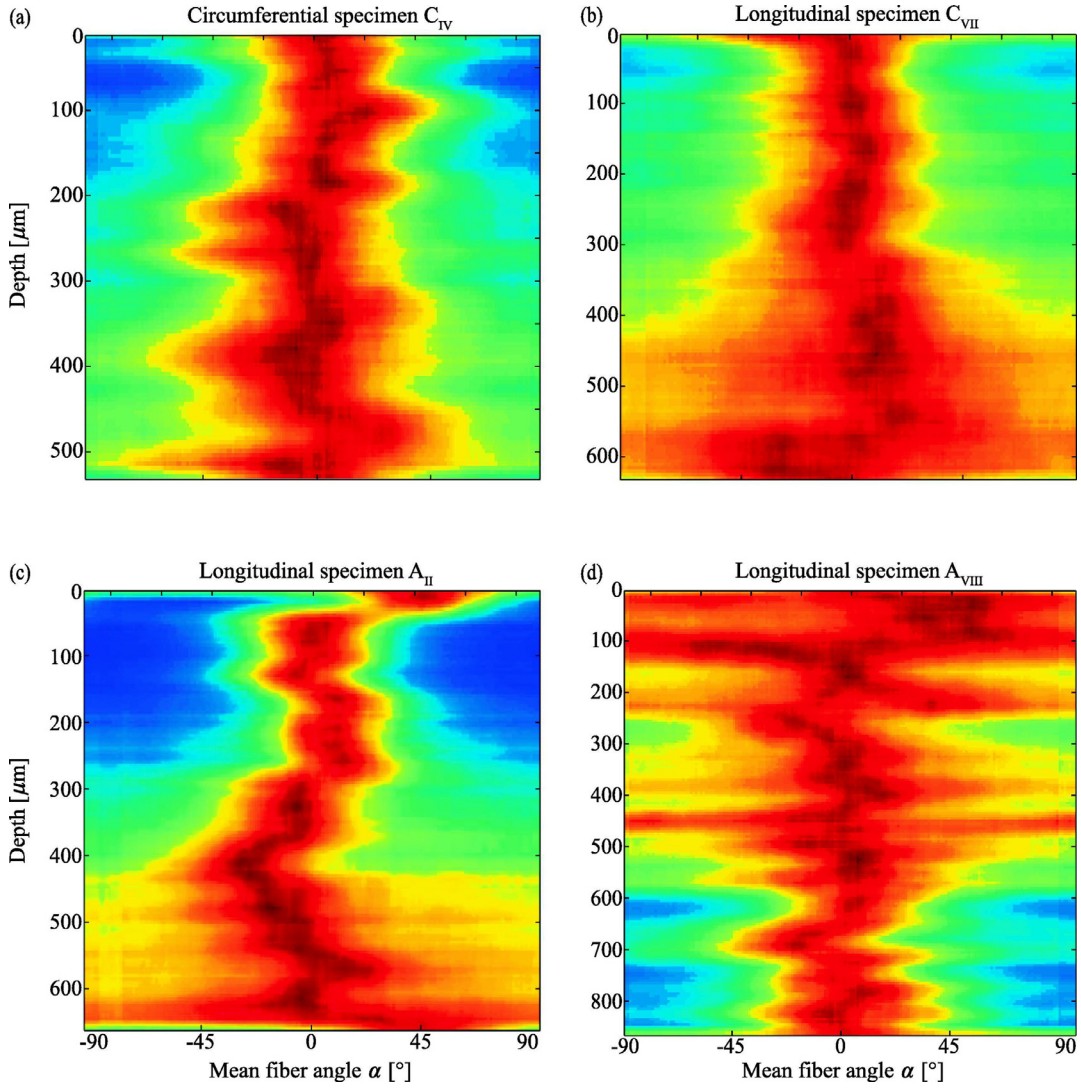

Fig. 7. Intensity plots for four specimens: (a) circumferential C_{IV} has highly aligned fibers along ±7° relative to the circumferential direction, with a dispersion parameter of $\kappa_{ip} = 0.20$; (b) longitudinal C_{VII} has aligned fibers along ±6°, with $\kappa_{ip} = 0.21$; (c) longitudinal A_{II} has aligned fibers along ±13°, with $\kappa_{ip} = 0.17$; (d) longitudinal A_{VIII} has fibers along ±14° with less alignment ($\kappa_{ip} = 0.22$) in comparison to (c). The abscissas refer to the angle measured from the circumferential direction at the origin (0°), while (±90°) refers to the longitudinal direction. The red color identifies angles at which there are fibers with that orientation, while the blue color indicates the absence of fibers.

4. Discussion

We have provided a unique set of data relating the uniaxial failure properties of aortic tissues to their microstructure, which shows that the tissue is able to carry higher loads when stretched in the mean fiber direction compared with the cross fiber direction, see Figs. 1 and 9, and Table 2. The general trend observed for the failure stresses (Control-C > Aneurysmatic-

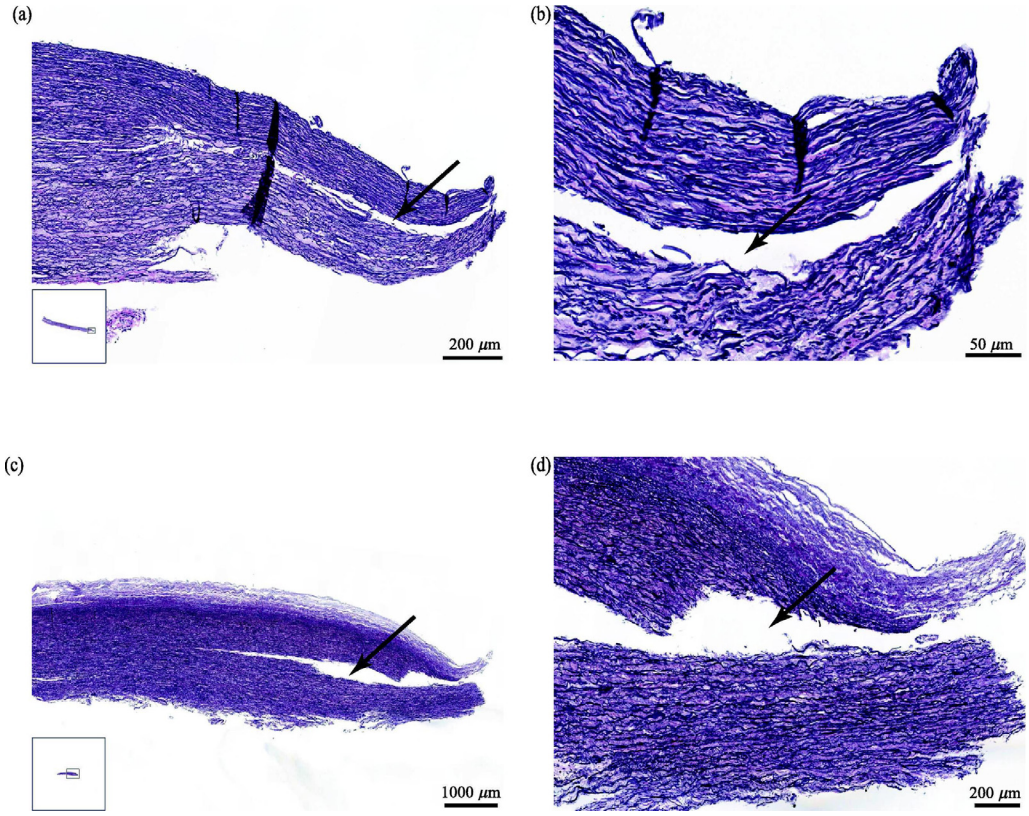

Fig. 8. Ruptured regions with black arrows indicating delaminations: (a) circumferential specimen A_{II} with a small delamination length of approximately 1.2 mm; (b) magnification of the delamination in (a); (c) circumferential specimen C_I with a rather long delamination of approximately 5.3 mm; (d) magnification of the delamination in (c).

C > Aneurysmatic-L > Control-L) was the opposite of that observed for the mean fiber angle from the loading direction (Control-L > Aneurysmatic-L > Aneurysmatic-C > Control-C). Fig. 9(a) confirms that tissue strips are stronger when the load is applied close to the mean fiber direction, while the failure stretch does not show any specific correlation with the mean fiber direction, see Fig. 9(b). Neither the failure stress nor stretch showed any clear correlation with the other structural parameters investigated herein. However, group trends indicate that in-plane fiber dispersion (Control-C > Aneurysmatic-C > Aneurysmatic-L > Control-L) and collagen content (Aneurysmatic-C > Control-C > Aneurysmatic-L > Control-L) also call for further discussion in relation to failure stresses (Control-C > Aneurysmatic-C > Aneurysmatic-L > Control-L) on the basis of specific cases.

4.1. Mechanics

4.1.1. Failure properties

With respect to Table 3 the mean failure stress from uniaxial extension tests of medias from the control group are higher in the circumferential than in the longitudinal direction (1474 versus 579 kPa). A higher mean failure stress in the circumferential than in the longitudinal direction was also found for intact healthy human thoracic aortas by Mohan & Melvin [35]

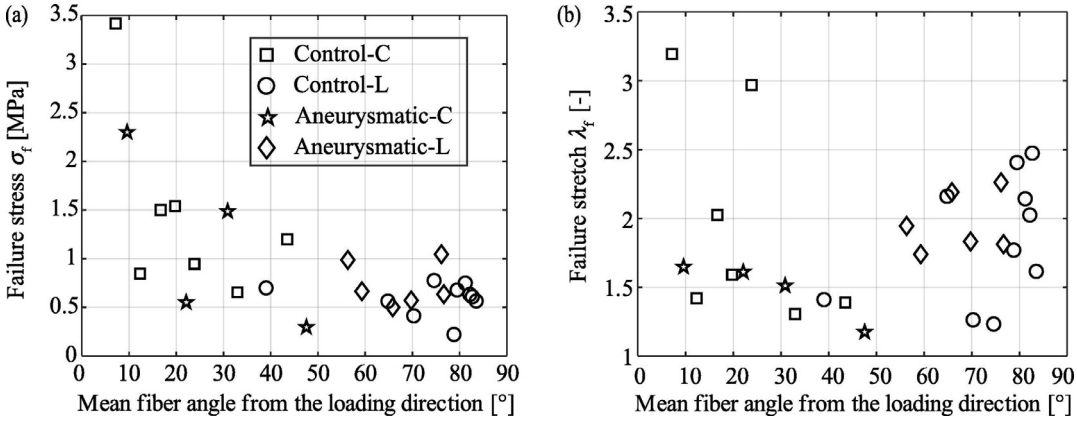

Fig. 9. Failure properties plotted against the mean fiber angle from the loading direction: (a) failure stress σ_f; (b) failure stretch λ_f.

(1720 versus 1470 kPa), Vorp et al. [36] (1800 versus 1710 kPa), and García-Herrera et al. [37] (2180 versus 1140 kPa), the latter being significantly different. The mean failure stress of the aneurysmatic media tested in the present study was also higher in the circumferential than in the longitudinal direction (1446 ± 875 versus 735 ± 227 kPa), but this difference was not significant. However, significantly different mean failure stresses of aneurysmatic human thoracic aortic medias in the circumferential and the longitudinal direction (1282 versus 565 kPa) were observed in a previous study by our group [31].

Several other studies also found higher failure stresses in the circumferential than in the longitudinal direction of the intact wall of human aneurysmatic thoracic aortas, i.e. 1190 versus 880 kPa in [37], 961 versus 540 kPa in [38], and 1440 versus 940 kPa in [39]. In contrast, the study [36] found almost isotropic failure properties of thoracic aortic aneurysms with similar mean failure stresses in the circumferential and longitudinal directions (1180 versus 1210 kPa). Most studies observed anisotropic failure stresses for healthy and aneurysmatic human thoracic aortic medias as well as for the intact wall, with higher stresses in the circumferential than in the longitudinal direction. The anisotropic failure stresses can be explained by the intrinsic collagen fiber assembly of the tissue, as illustrated in Fig. 1.

Interestingly, mean failure stretches of the thoracic aortic media were determined to be similar in the circumferential and longitudinal direction for the aneurysmatic group (1.59 versus 1.6) but different for the control group (2.18 versus 1.9). In contrast, failure stretches of the intact healthy human thoracic aortic wall were found to be smaller in the circumferential than in the longitudinal direction (1.23 versus 1.47) [35]. Failure stretches of human aneurysmatic thoracic aortas were found to be the same in both directions (1.52 versus 1.52) for the media [31] and for the intact wall (1.34 versus 1.34) [39], but also larger in the circumferential than in the longitudinal direction (1.61 versus 1.47) [38].

Specimens investigated in this study exhibited a wide range of failure stresses and stretches, and these values were not correlated. The aneurysm diameter was not found to be correlated with failure properties. This may in part be explained by donors who may have slowly growing stable aneurysms, and the load that the specimen can withstand at different stretches can be very different, as can be seen from Fig. 6.

4.1.2. Definition of failure

It is important to note that the definition of the failure point differs between the above mentioned studies and the present study. Hence care must be taken when interpreting a failure point. We define the failure stress as the Cauchy stress at maximum force the tissue is able to carry, and the Cauchy stress-stretch curves end at this value. After the maximum force, there was either full or partial separation, and in the latter case the specimen was still able to carry load at a decreased capacity until full separation occurred. The studies [31,35,36,38,39] defined the failure point as the point where the maximum Cauchy stress occurs prior to failure. In the present study, only two specimens showed a difference larger than 1% between these two definitions of failure, in particular 8% and 4% for circumferential C_{IX} and longitudinal C_{XII}, respectively.

On the other hand, the study [37] defined the failure point as the first point where one of the layers failed, which relates to a sudden drop in the Cauchy stress-stretch curve. In our study, we observed several of these sudden drops even at a rather low stress level but these specimens were still able to withstand much higher stresses to failure. Consequently, local failure may have already occurred at these sudden drops before the maximum force value is reached. In addition, for example, the specimens C_{IV} in Fig. 5 and A_V in Fig. 5(d) exhibit changes in the slope of the stress-stretch curve but not sharp inflections. Recent studies reported that a change in the stress-stretch slope is related to damage accumulation in collagen molecules [40,41].

4.2. Microstructure

The higher values of the out-of-plane dispersion parameters κ_{op}^{rz} and $\kappa_{op}^{r\theta}$ of the control group indicate that the fibers are more aligned within the lamellar units in the control group than in the aneurysmatic group, similarly to that found for abdominal aortic aneurysms [42]. The in-plane structural parameter κ_{ip} of the specimens investigated were not significantly different between the two groups, which is also in agreement with that found for human abdominal aortas [42]. Moreover, histological investigations showed that the collagen, elastic fiber and SMC content was not significantly different between the two groups (Table 4), and the same tendency was observed between all four groups (Table 3). The aforementioned similarities and differences do not necessarily indicate the absence or existence of structural changes due to aneurysm formation. They could also result from the anamnesis of the donors such as age, imperfect layer separation, imaging after testing and different sections of the aorta investigated herein. Moreover, the structure of the specimens obtained from donors who had suffered from tumors may not correspond to healthy structure, as arterial stiffening has been reported in cancer patients [43–45].

4.3. Uniaxial failure properties and microstructure

4.3.1. Influence of the fiber angle relative to the loading direction

We observed an inverse relationship between the failure stress σ_f and the mean fiber angle relative to the loading direction, as depicted in Fig. 9(a). Specifically, the higher the mean fiber angle from the loading direction the lower the failure stress. Further investigation is needed to clarify the possible influence of the structural parameters other than the mean fiber direction even though the failure properties did not show any clear dependencies on these parameters.

With respect to Table 2, the circumferential specimen C_{IV} showed the highest failure stress ($\sigma_f = 3418$ kPa) and the lowest mean fiber angle α (7°). It is likely that this very high failure stress is not only a result of the mean fiber angle but also due to the presence of the adventitia (20% of the thickness). It is well accepted that the adventitia acts as a protective layer against tissue failure due to its high collagen content. This specimen revealed also the highest failure stretch ($\lambda_f = 3.20$), which may in part be explained by the waviness of the collagen fibers in the unloaded state.

The longitudinal specimen C_I revealed the lowest failure stress ($\sigma_f = 222$ kPa) and a high mean fiber angle relative to the loading direction (79°). The highest mean fiber angle relative to the loading direction (84°) was identified for the longitudinal specimen C_{VII} with a failure stress of $\sigma_f = 566$ kPa. The higher failure stress of C_{VII} might be explained by the slightly more aligned out-of-plane structure indicated by the values of κ_{op}^{rz}, and the higher collagen and elastic fiber content since both specimens have similar κ_{ip} values; see Table 2.

4.3.2. Influence of collagen and elastic fiber contents

Consider now the circumferential specimens A_{IX} ($\sigma_f = 552$ kPa, $\lambda_f = 1.61, \alpha = 22°, \kappa_{ip} = 0.26$, 50% collagen) and A_{III} ($\sigma_f = 1487$ kPa, $\lambda_f = 1.51, \alpha = 31°, \kappa_{ip} = 0.29$, 25% collagen). These two specimens suggest that an increased collagen content correlates with lower failure stress but this is counterintuitive in the sense that it might be expected that higher collagen content would increase

the strength due to the increased reinforcement. However, the presence of the intima in the circumferential specimen A_{IX} (16%), may have reduced the failure stress. In addition, the high percentage of the collagen and the low percentage of elastic fiber content may lead to premature failure by limiting the extensibility of the tissue [46], as in the case of the circumferential specimen A_I ($\sigma_f = 297$ kPa, $\lambda_f = 1.17, \alpha = 48°, \kappa_{ip} = 0.28$ and 70% collagen).

4.3.3. Influence of fiber dispersion

The longitudinal specimens A_{II} and A_{VIII} show very different failure stress values σ_f, 636 and 1046 kPa, respectively, despite similar values for the mean fiber angle and $\kappa_{op}^{r\theta}$, and the same values for κ_{op}^{rz} and the content percentages. Since they consist of only the media they provide a good basis for discussing the influence of the κ_{ip} values on the failure stress. Fig. 7(c) and (d) depict the in-plane fiber distributions of A_{II} ($\alpha = 13°, \kappa_{ip} = 0.17$, 100% media), and A_{VIII} ($\alpha = 14°, \kappa_{ip} = 0.22$, 100% media), respectively. The more aligned the fibers are in a direction further away from the loading direction, in this case the longitudinal direction, the lower is the possibility of finding fibers which will be able to support the load, and hence the lower failure stress for the specimen A_{II}.

Note that the mean fiber angle and the dispersion parameter κ_{ip} have a considerable influence on the failure stress, hence the dispersion parameter κ_{ip} should not be omitted from constitutive formulations.

4.3.4. Other influences

There are some data points in Fig. 9(a) that have similar failure stresses but different mean fiber angles. For example, by comparing the circumferential specimen C_{VIII} ($\alpha = 33°, \kappa_{ip} = 0.23$) to the longitudinal specimen C_{XII} ($\alpha = 8°, \kappa_{ip} = 0.23$) and the longitudinal specimen A_{VII} ($\alpha = 31°, \kappa_{ip} = 0.18$), one would expect that the specimen C_{VIII} exhibits the highest failure stress σ_f followed by A_{VII} and C_{XII}, which is not the case. These specimens have similar content percentages, and hence one explanation for the lower failure stress for C_{VIII} being unexpected is the decreased fibrillar reinforcement due to the presence of the intimal collagen, and the presence of adventitial collagen in the other two specimens.

Although we did not investigate the influence of substructures such as collagen cross-links, their effect on the uniaxial failure properties σ_f and λ_f could be significant. The longitudinal specimen C_I with the lowest failure stress has very similar values of the structural parameters to those of the longitudinal specimen C_{II}. However, the specimen C_{II} has a much higher failure stress ($\sigma_f = 679$ kPa). As indicated in Table 1, donor C_I passed away due to myocardial infarction whereas donor C_{II} passed away due to tumor progression. The substructures of the aortic wall of C_I might be significantly different than those of C_{II} resulting in a decreased extensibility and a lower failure stress. Disruptions to the lamellar organization in the rupture zone of specimen C_I when compared to the neatly packed rupture zone of specimen C_{II}, as depicted in Fig. 4(a) and (b), indicate that the interlamellar connections likely play a significant role.

Although the mean fiber direction has a clear influence on the failure stress σ_f, it is not the only parameter that should be taken into account when modeling failure properties. As discussed above, the values of the dispersion parameters and the collagen and elastic fiber content seem to have a considerable influence on the failure stress. Although their combined effects are not obvious to assess and are difficult to estimate, all these parameters should be considered when attempting to model failure of soft collagenous tissues.

4.4. Rupture zone

The rupture zone is characterized by ruptured collagen and elastic fibers. In some specimens delamination of the lamellas was also visible. The cracks, as illustrated in Fig. 8, were also observed in [47] under uniaxial tensile loading combined with X-ray microtomography, and suggest that failure initiation and propagation are complex mechanisms. Fig. 8 shows ruptured collagen and elastic fibers at the rupture ends, as expected under loading. In addition, the delamination areas visible in Fig. 8(a)–(d) suggest that both interfiber collagen cross-links and interlamellar cross-links are broken.

Although the specimens are stretched along their main axes, the fibers which are not perfectly aligned with these axes may enhance the effect of shear which contributes to delamination. In the study [48] pulsatile pressure experiments were performed. The authors concluded that cracks between the lamellas indicate that shearing mechanisms are involved in the process, and the follow-up study [49] concluded that the links between the lamellas are weaker than the lamellas themselves, which leads to the cracks between them. The study [50] suggested that collagen fiber pull-out from the matrix and peeling-like processes also result in broken bonds between the collagen fibers, and therefore play an important role. In addition, interfiber cross-links are possibly under higher tension than they can sustain, which also contributes to delamination [51,52]. Based on the experimental observations in [47], the study in [53] investigated the effects of shear delamination strength on tissue failure under uniaxial loading by means of finite element analyses. The authors concluded that local wall defects may contribute directly to the initiation of dissection by reducing the shear delamination strength.

The aforementioned studies used different experimental methods, but resulted in similar histological observations to those presented here. Although we cannot identify the initial failure zone, as imaging and loading were not performed simultaneously, the delamination zones suggest that not only the collagen fiber architecture but also the different types of cross-links should be considered while attempting to model soft tissue failure under uniaxial extension loading.

4.5. Limitations

Due to the small sizes of the donor samples especially the aneurysmatic ones, it was not always possible to obtain circumferential and longitudinal data for each sample. Hence, we have not provided extensive details of the anisotropy. Regions with alterations such as calcification and atherosclerosis were not suitable for our investigations, thus reducing the amount of tissue available for testing. In addition, some tests failed as the rupture occurred outside the markers instead of within the gauge region. Where there was more tissue available in a sample, more specimens were prepared for testing. This also resulted in small and unmatched group sizes making it difficult to generalize the findings of the study.

The conditions from explantation to arrival were different between donor samples, and all samples were frozen until testing, as mentioned in Section 2. The mechanics of the biological tissues may be influenced by the duration of freezing, solution they were kept in, and the rates of freezing and thawing due to osmotic pressure imbalances and intracellular ice formation [54–56]. Solutions such as Ringer's lactate [57] and PBS [58] have been shown to help preserve the mechanical properties. Furthermore, the use of DMSO reduces the intracellular ice formation due to freezing [56], although the effect is concentration dependent [55]. It is assumed, therefore, that the influence of different solutions and duration of

freezing on the mechanical properties is negligible. Regardless, cell functionality may still be damaged during thawing [56]. Aortic endothelial and smooth muscle cells, for example, are reported to significantly lose their functionality due to thawing, but no significant influences are observed for the aortic mechanics [59]. Such damage to cell functionality creates desirable effects in fact, and are discussed later.

Arteries are residually stressed in both circumferential and longitudinal directions *in vivo*, for which elastin is mainly responsible for [60]. When an unloaded arterial ring is cut radially, it springs open and a longitudinal strip bends further away from the main vessel axis due to the release of stresses. As the donor samples were either received in several pieces or as a ring which was then cut open during preparation, residual stresses were partially released. Furthermore, residual stresses also depend on the contraction state of the SMCs, i.e. the basal tone [61]. However, SMC functionality is likely to be significantly impaired due to thermal injury, as discussed before, which further reduces the possible influence of residual stresses.

As the histological investigations revealed, layer separation was not complete for all specimens, and the uniaxial testing data of a particular specimen does not necessarily reflect the mechanical behavior of the media alone. Since the residual stresses are layer dependent [62], they may have an influence on the uniaxial failure properties of these specimens.

The structural similarities and differences between the control and aneurysmatic groups might arise from the different aortic segments which were available for this study, in addition to the donor anamnesis. It is assumed here that the differences in the uniaxial failure properties between the different regions and age groups are due to the microstructural differences [63]. Nevertheless, such differences may be present for various components at different length scales not investigated herein. Furthermore, the SHG images were obtained from the ruptured specimens without accounting for the fiber reorientation and recoil after failure. This might also explain some of the scatter of the data points presented in Fig. 9(a) and (b).

The present study and the studies cited in Section 4.1 employed quasi-static deformation rates. However, the aorta is reported to be significantly stronger under dynamic deformation rates [35], so that the influence of the microstructure on the time-dependent failure properties needs to be further investigated. Nevertheless, the identification of failure properties under quasi-static uniaxial extension, and the influence of the microstructure on these properties constitute an important step towards the development of a more realistic failure criterion for soft biological tissues. Another limitation is the use of uniaxial extension tests instead of biaxial tests as the latter would provide a more realistic estimation of the *in vivo* stresses in the aortic wall when dilated due to aneurysm or dissection. However, to our knowledge, there are no reliable planar biaxial testing methods available for obtaining failure properties. On the other hand, bulge inflation tests were employed in several studies, and the findings also indicate the important role the microstructure plays in tissue failure [46,64,65].

5. Conclusions

The present study provides a unique set of mechanical and structural data that highlight the strong influence of the aortic media microstructure on its failure properties under uniaxial extension loading. The data presented show that not only the mean collagen fiber angle from the loading direction, but also the dispersion has a clear influence on the failure properties of the specimens subjected to uniaxial extension. Furthermore, contents of collagen and elastic fibers should also be considered – specially in the cases where they are extremely high/low. It would be of interest to investigate the influence of the microstructure on the failure properties under different loading modes, isolated and mixed. Such investigations could help predict not only when the dilated wall is likely to rupture, but also when an aorta (aneurysmatic or apparently healthy) might develop a dissection. More research is required in order to characterize the interlamellar strength under different loading modes, and the influence of the microstructure on the strength to inform the prediction of possible dissection.

In line with recent studies on aortic tissue [66] and bovine pericardium [67], the results of this work suggest that the microstructure should be taken into account when developing failure criteria. This study should be considered as a basis for further research that focus on the predictive capabilities of the microstructural parameters for the failure properties of soft biological tissues, and it is a step towards realistic modeling of tissue failure. In addition, it might help to address clinical challenges of rupture prediction of dilated aortas with appropriate imaging techniques.

Declaration of Competing Interest

The authors declare that they have no known competing financial interests or personal relationships that could have appeared to influence the work reported in this paper.

Acknowledgement

The authors are indebted to Dr. Heimo Wolinski, Yeast Genetics and Molecular Biology Group, University of Graz, for his support during SHG imaging; to Augustin Donnerer, Diagnostic and Research Institute of Pathology, Medical University of Graz, for his support in collecting the control samples; to Dr. Otto Dapunt and Dr. Peter Oberwalder, Division of Cardiac Surgery, Medical University Graz, for providing the diseased sample A_I. Furthermore, we gratefully acknowledge the financial support of the National Institutes of Health (NIH), research Grant No. NIH R01HL117063. In addition, this work was partly supported by the Lead Project on 'Mechanics, Modeling and Simulation of Aortic Dissection', granted by 575 Graz University of Technology, Austria. The work of R.W.O. was, in part, funded by the UK EPSRC Grant No. EP/N014642/1.

References

[1] C. Olsson, S. Thelin, E. Ståhle, A. Ekbom, F. Granath, Thoracic aortic aneurysm and dissection: increasing prevalence and improved outcomes reported in a nationwide population-based study of more than 14,000 cases from to 2002, Circulation 114 (2006) (1987) 2611–2618.
[2] L.G. Svensson, N.T. Kouchoukos, D.C. Miller, J.E. Bavaria, J.S. Coselli, M.A. Curi, H. Eggebrecht, J.A. Elefteriades, R. Erbel, T.G. Gleason, B.W. Lytle, R.S. Mitchell, C.A. Nienaber, E.E. Roselli, H.J. Safi, R.J. Shemin, G.A. Sicard, T.M. Sundt 3rd, W.Y. Szeto, G.H. Wheatley 3rd, Society of Thoracic Surgeons Endovascular Surgery Task Force, Expert consensus document on the treatment of descending thoracic aortic disease using endovascular stent-grafts, Ann. Thorac. Surg. 85 (2008) S1–S41.
[3] L.A. Pape, M. Awais, E.M. Woznicki, T. Suzuki, S. Trimarchi, A. Evangelista, T. Myrmel, M. Larsen, K.M. Harris, K. Greason, M. Di Eusanio Bossone, D.G. Montgomery, K.A. Eagle, C.A. Nienaber, E.M. Isselbacher, P. O'Gara, Presentation diagnosis, and outcomes of acute aortic dissection: 17-year trends from the international registry of acute aortic dissection, J. Am. Coll. Cardiol. 66 (2015) 350–358.
[4] F.A. Lederle, S.E. Wilson, G.R. Johnson, D.B. Reinke, F.N. Littooy, C.W. Acher, D.J. Ballard, L.M. Messina, I.L. Gordon, E.P. Chute, W.C. Krupski, S.J. Busuttil, G.W. Barone, S. Sparks, L.M. Graham, J.H. Rapp, M.S. Makaroun, G.L. Moneta, R.A. Cambria, R.G. Makhoul, D. Eton, H.J. Ansel, J.A. Freischlag, D. Bandyk, Aneurysm Detection and Management Veterans Affairs Cooperative Study Group, Immediate repair compared with surveillance of small abdominal aortic aneurysms, N. Engl. J. Med. 346 (2002) 1437–1444.
[5] S.O. Hansson, Implant ethics, J. Med. Ethics 31 (2005) 519–525.
[6] N. Grootenboer, J.L. Bosch, J.M. Hendriks, M.R. van Sambeek, Epidemiology, aetiology, risk of rupture and treatment of abdominal aortic aneurysms: does sex matter? Eur. J. Vasc. Endovasc. Surg. 38 (2009) 278–284.
[7] J.B. Kim, K. Kim, M.E. Lindsay, T. MacGillivray, E.M. Isselbacher, R.P. Cambria, T.M. Sundt, Risk of rupture or dissection in descending thoracic aortic aneurysm, Circulation 132 (2015) 1620–1629.

[8] L.A. Pape, T.T. Tsai, E.M. Isselbacher, J.K. Oh, P.T. O'Gara, A. Evangelista, R. Fattori, G. Meinhardt, S. Trimarchi, E. Bossone, T. Suzuki, J.V. Cooper, J.B. Froehlich, C.A. Nienaber, K.A. Eagle, International Registry of Acute Aortic Dissection (IRAD) Investigators, Aortic diameter > or = 5.5 cm is not a good predictor of type A aortic dissection: Observations from the International Registry of Acute Aortic Dissection (IRAD), Circulation 116 (2007) 1120–1127.

[9] N. Choudhury, O. Bouchot, L. Rouleau, D. Tremblay, R. Cartier, J. Butany, R. Mongrain, R.L. Leask, Local mechanical and structural properties of healthy and diseased human ascending aorta tissue, Cardiovasc. Pathol. 18 (2009) 83–91.

[10] G.A. Holzapfel, T.C. Gasser, R.W. Ogden, A new constitutive framework for arterial wall mechanics and a comparative study of material models, J. Elasticity 61 (2000) 1–48.

[11] G.A. Holzapfel, G. Sommer, C.T. Gasser, P. Regitnig, Determination of layer-specific mechanical properties of human coronary arteries with non-atherosclerotic intimal thickening, and related constitutive modeling, Am. J. Physiol. Heart Circ. Physiol. 289 (2005) H2048–2058.

[12] F.H. Silver, D.L. Christiansen, C.M. Buntin, Mechanical properties of the aorta: a review, Crit. Rev. Biomed. Eng. 17 (1989) 323–358.

[13] A. Karimi, D.M. Milewicz, Structure of the elastin-contractile units in the thoracic aorta and how genes that cause thoracic aortic aneurysms and dissections disrupt this structure, Canad. J. Cardiol. 32 (2016) 26–34.

[14] M.K. O'Connell, S. Murthy, S. Phan, C. Xu, J. Buchanan, R. Spilker, R.L. Dalman, C.K. Zarins, W. Denk, C.A. Taylor, The three-dimensional micro- and nanostructure of the aortic medial lamellar unit measured using 3D confocal and electron microscopy imaging, Matrix Biol. 27 (2008) 171–181.

[15] K. von der Mark, Localization of collagen types in tissues, Int. Rev. Conn. Tiss. Res. 9 (1981) 265–324.

[16] A.J. Schriefl, G. Zeindlinger, D.M. Pierce, P. Regitnig, G.A. Holzapfel, Determination of the layer-specific distributed collagen fiber orientations in human thoracic and abdominal aortas and common iliac arteries, J.R. Soc. Interface 9 (2012) 1275–1286.

[17] J. Erdheim, Medionecrosis aortae idiopathica, Virch. Arch. Pathol. Anat. 273 (1929) 454–479.

[18] S. Bode-Jänisch, A. Schmidt, D. Günther, M. Stuhrmann, A. Fieguth, Aortic dissecting aneurysms – histopathological findings, Forensic. Sci. Int. 214 (2012) 13–17.

[19] J.D. Humphrey, Possible mechanical roles of glycosaminoglycans in thoracic aortic dissection and associations with dysregulated transforming growth factor-β, J. Vasc. Res. 50 (2013) 1–10.

[20] D. Wu, Y.H. Shen, L. Russell, J.S. Coselli, S.A. LeMaire, Molecular mechanisms of thoracic aortic dissection, J. Surg. Res. 184 (2013) 907–924.

[21] L.F. Borges, J.P.F. Blini, R.R. Dias, P.S. Gutierrez, Why do aortas cleave or dilate? Clues from an electronic scanning microscopy study in human ascending aortas, J. Vasc. Res. 51 (2014) 50–57.

[22] J.A. Jones, C. Beck, J.R. Barbour, J.A. Zavadzkas, R. Mukherjee, F.G. Spinale, J.S. Ikonomidis, Alterations in aortic cellular constituents during thoracic aortic aneurysm development: myofibroblast-mediated vascular remodeling, Am. J. Pathol. 175 (2009) 1746–1756.

[23] L.F. Borges, R.G. Jaldin, R.R. Dias, N.A. Stolf, J.B. Michel, P.S. Gutierrez, Collagen is reduced and disrupted in human aneurysms and dissections of ascending aorta, Hum. Pathol. 39 (2008) 437–443.

[24] X. Wang, S.A. LeMaire, L. Chen, Y.H. Shen, Y. Gan, H. Bartsch, S.A. Carter, B. Utama, H. Ou, J.S. Coselli, X.L. Wang, Increased collagen deposition and elevated expression of connective tissue growth factor in human thoracic aortic dissection, Circulation 114 (2006) I–200–I–205.

[25] B.L.Y. Cheuk, S.W.K. Cheng, Differential expression of elastin assembly genes in patients with Stanford Type A aortic dissection using microarray analysis, J. Vasc. Surg. 53 (2011) 1071–1078.

[26] L. Wang, J. Zhang, W. Fu, D. Guo, J. Jiang, Y. Wang, Association of smooth muscle cell phenotypes with extracellular matrix disorders in thoracic aortic dissection, J. Vasc. Surg. 56 (2012) 1698–1709.

[27] G.A. Holzapfel, G. Sommer, P. Regitnig, Anisotropic mechanical properties of tissue components in human atherosclerotic plaques, J. Biomech. Eng. 126 (2004) 657–665.

[28] G. Sommer, C. Benedikt, J.A. Niestrawska, G. Hohenberger, C. Viertler, P. Regitnig, T.U. Cohnert, G.A. Holzapfel, Mechanical response of human subclavian and iliac arteries to extension, inflation and torsion, Acta Biomater. 75 (2018) 235–252.

[29] G. Sommer, M. Eder, L. Kovacs, H. Pathak, L. Bonitz, C. Mueller, P. Regitnig, G.A. Holzapfel, Multiaxial mechanical properties and constitutive modeling of human adipose tissue: a basis for preoperative simulations in plastic and reconstructive surgery, Acta Biomater. 9 (2013) 9036–9048.

[30] G. Sommer, A. Schriefl, G. Zeindlinger, A. Katzensteiner, H. Ainödhofer, A. Saxena, G.A. Holzapfel, Multiaxial mechanical response and constitutive modeling of esophageal tissues: impact on esophageal tissue engineering, Acta Biomater. 9 (2013) 9379–9091.

[31] G. Sommer, S. Sherifova, P.J. Oberwalder, O.E. Dapunt, P.A. Ursomanno, A. DeAnda, B.E. Griffith, G.A. Holzapfel, Mechanical strength of aneurysmatic and dissected human thoracic aortas at different shear loading modes, J. Biomech. 49 (2016) 2374–2382.

[32] A.J. Schriefl, H. Wolinski, P. Regitnig, S.D. Kohlwein, G.A. Holzapfel, An automated approach for three-dimensional quantification of fibrillar structures in optically cleared soft biological tissues, J.R. Soc. Interface 10 (2013) 20120760.

[33] G.A. Holzapfel, J.A. Niestrawska, R.W. Ogden, A.J. Reinisch, A.J. Schriefl, Modelling non-symmetric collagen fibre dispersion in arterial walls, J.R. Soc. Interface 12 (2015) 20150188.

[34] B. Alberts, A. Johnson, J. Lewis, D. Morgan, M. Raff, K. Roberts, P. Walter, Molecular Biology of the Cell, 6th ed., Garland Science, New York, 2015.

[35] D. Mohan, J.W. Melvin, Failure properties of passive human aortic tissue. I – uniaxial tension tests, J. Biomech. 15 (1982) 887–902.

[36] D.A. Vorp, B.J. Schiro, M.P. Ehrlich, T.S. Juvonen, M.A. Ergin, B.P. Griffith, Effect of aneurysm on the tensile strength and biomechanical behavior of the ascending thoracic aorta, Ann. Thorac. Surg. 800 (2003) 1210–1214.

[37] C.M. García-Herrera, J.M. Atienza, F.J. Rojo, E. Claes, G.V. Guinea, D.J. Celentano, C. García-Montero, R.L. Burgos, Mechanical behaviour and rupture of normal and pathological human ascending aortic wall, Med. Biol. Eng. Comput. 50 (2012) 559–566.

[38] J.E. Pichamuthu, J.A. Phillippi, D.A. Cleary, D.W. Chew, J. Hempel, D.A. Vorp, T.G. Gleason, Differential tensile strength and collagen composition in ascending aortic aneurysms by aortic valve phenotype, Ann. Thorac. Surg. 96 (2013) 2147–2154.

[39] A. Ferrara, S. Morganti, P. Totaro, A. Mazzola, F. Auricchio, Human dilated ascending aorta: Mechanical characterization via uniaxial tensile tests, J. Mech. Behav. Biomed. Mater. 53 (2016) 257–271.

[40] M.I. Converse, R.G. Walther, J.T. Ingram, Y. Li, S.M. Yu, K.L. Monson, Detection and characterization of molecular-level collagen damage in overstretched cerebral arteries, Acta Biomater. 67 (2018) 307–318.

[41] M. Marino, M.I. Converse, K.L. Monson, P. Wriggers, Molecular-level collagen damage explains softening and failure of arterial tissues: a quantitative interpretation of CHP data with a novel elasto-damage model, J. Mech. Behav. Biomed. Mater. 97 (2019) 254–271.

[42] J.A. Niestrawska, C. Viertler, P. Regitnig, T.U. Cohnert, G. Sommer, G.A. Holzapfel, Microstructure and mechanics of healthy and aneurysmatic abdominal aortas: experimental analysis and modeling, J.R. Soc. Interface 13 (2016) 20160620.

[43] M. Alivon, J. Giroux, M. Briet, F. Goldwasser, S. Laurent, P. Boutouyrie, Large artery stiffness and hypertension after antiangiogenic drugs: influence on cancer progression, J. Hypertension 33 (2015) 1310–1317.

[44] S. Grover, P.W. Lou, C. Bradbrook, K. Cheong, D. Kotasek, D.P. Leong, B. Koczwara, J.B. Selvanayagam, Early and late changes in markers of aortic stiffness with breast cancer therapy, Intern. Med. J. 45 (2015) 140–147.

[45] I. Mozos, G. Borzak, A. Caraba, R. Mihaescu, Arterial stiffness in hematologic malignancies, OncoTargets Ther. 10 (2017) 1381–1388.

[46] R. Pearson, N. Philips, R. Hancock, S. Hashim, M. Field, D. Richens, D. McNally, Regional wall mechanics and blunt traumatic aortic rupture at the isthmus, Eur. J. Cardiothorac. Surg. 34 (2008) 616–622.

[47] C. Helfenstein-Didier, D. Taïnoff, J. Viville, J. Adrien, É. Maire, P. Badel, Tensile rupture of medial arterial tissue studied by X-ray micro-tomography on stained samples, J. Mech. Behav. Biomed. Mater. 78 (2018) 362–368.

[48] C. van Baardwijk, M.R. Roach, Factors in the propagation of aortic dissection in canine thoracic aortas, J. Biomech. 20 (1987) 67–73.

[49] M.W. Carson, M.R. Roach, The strength of the aortic media and its role in the propagation of aortic dissection, J. Biomech. 23 (1990) 579–588.

[50] H.W. Haslach Jr., P. Riley, A. Molotsky, The influence of medial substructures on rupture in bovine aortas, Cardiovasc. Eng. Technol. 2 (2011) 372–387.

[51] H.W. Haslach Jr., L.N. Leahy, P. Fathi, J.M. Barrett, A.E. Heyes, T.A. Dumsha, E.L. McMahon, Crack propagation and its shear mechanisms in the bovine descending aorta, Cardiovasc. Eng. Technol. 6 (2015) 501–518.

[52] H.W. Haslach Jr., A. Siddiqui, A. Weerasooriya, R. Nguyen, J. Roshgadol, N. Monforte, E. McMahon, Fracture mechanics of shear crack propagation and dissection in the healthy bovine descending aortic media, Acta Biomater. 68 (2018) 53–66.

[53] J. Brunet, B. Pierrat, E. Maire, J. Adrien, P. Badel, A combined experimental-numerical lamellar-scale approach of tensile rupture in arterial medial tissue using X-ray tomography, J. Mech. Behav. Biomed. Mater. 95 (2019) 116–123.

[54] L.E. McGann, H.Y. Yang, M. Walterson, Manifestations of cell damage after freezing and thawing, Cryobiology 25 (1988) 178–185.

[55] Y. Xu, T.C. Hua, D.W. Sun, G.Y. Zhou, F. Xu, Effects of freezing rates and dimethyl sulfoxide concentrations on thermal expansion of rabbit aorta during freezing phase change as measured by thermo mechanical analysis, J. Biomech. 40 (2007) 3201–3206.

[56] E. Müller-Schweinitzer, Cryopreservation of vascular tissues, Organogenesis 5 (2009) 97–104.

[57] B.D. Stemper, N. Yoganandan, M.R. Stineman, T.A. Gennarelli, J.L. Baisden, F.A. Pintar, Mechanics of fresh, refrigerated, and frozen arterial tissue, J. Surg. Res. 139 (2007) 236–242.

[58] M. Adham, J.P. Gournier, J.P. Favre, E. De La Roche, C. Ducerf, J. Baulieux, X. Barral, M. Pouyet, Mechanical characteristics of fresh and frozen human descending thoracic aorta, J. Surg. Res. 64 (1996) 32–34.

[59] S.E. Langerak, M. Groenink, E.E. van der Wall, C. Wassenaar, E. Vanbavel, M.C. van Baal, J.A.E. Spaan, Impact of current cryopreservation procedures on mechanical and functional properties of human aortic homografts, Transpl. Int. 14 (2001) 248–255.

[60] A. Saini, C. Berry, S. Greenwald, Effect of age and sex on residual stress in the aorta, J. Vasc. Res. 32 (1995) 398–405.

[61] T. Matsumoto, M. Tsuchida, M. Sato, Change in intramural strain distribution in rat aorta due to smooth muscle contraction and relaxation, Am. J. Physiol. Heart Circ. Physiol. 271 (1996) H1711–H1716.

[62] S.E. Greenwald, J.E. Moore Jr., A. Rachev, T.P.C. Kane, J.-J. Meister, Experimental investigation of the distribution of residual strains in the artery wall, J. Biomech. Eng. 119 (1997) 438–444.
[63] D. Haskett, G. Johnson, A. Zhou, U. Utzinger, J. Vande Geest, Microstructural and biomechanical alterations of the human aorta as a function of age and location, Biomech. Model. Mechanobiol. 9 (2010) 725–736.
[64] Y. Luo, A. Duprey, S. Avril, J. Lu, Characteristics of thoracic aortic aneurysm rupture in vitro, Acta Biomater. 42 (2016) 286–295.
[65] A. Duprey, O. Trabelsi, M. Vola, J.P. Favre, S. Avril, Biaxial rupture properties of ascending thoracic aortic aneurysms, Acta Biomater. 42 (2016) 273–285.
[66] J.R. Thunes, J.A. Phillippi, T.G. Gleason, D.A. Vorp, S. Maiti, Structural modeling reveals microstructure-strength relationship for human ascending thoracic aorta, J. Bioeng. 71 (2018) 84–93.
[67] A. Whelan, J. Duffy, R.T. Gaul, D. O'Reilly, D.R. Nolan, P. Gunning, C. Lally, B.P. Murphy, Collagen fibre orientation and dispersion govern ultimate tensile strength, stiffness and the fatigue performance of bovine pericardium, J. Mech. Behav. Biomed. Mater. 90 (2019) 54–60.